Inorg. Chem. **2004**, *43*, 1625–1637

Nature of the Oxomolybdenum–Thiolate π-Bond: Implications for Mo–S Bonding in Sulfite Oxidase and Xanthine Oxidase

Rebecca L. McNaughton,[†] Matthew E. Helton,[†] Michele Mader Cosper,[‡] John H. Enemark,*[,‡] and Martin L. Kirk*[,†]

Departments of Chemistry, The University of New Mexico, MSC03 2060, 1 University of New Mexico, Albuquerque, New Mexico 87131-0001, and University of Arizona, Tucson, Arizona 85721

Received February 24, 2003

The electronic structure of *cis*,*trans*-(L-N_2S_2)MoO(X) (where L-N_2S_2 = *N*,*N*′-dimethyl-*N*,*N*′-bis(2-mercaptophenyl)-ethylenediamine and X = Cl, $SCH_2C_6H_5$, SC_6H_4–OCH_3, or $SC_6H_4CF_3$) has been probed by electronic absorption, magnetic circular dichroism, and resonance Raman spectroscopies to determine the nature of oxomolybdenum–thiolate bonding in complexes possessing three equatorial sulfur ligands. One of the phenyl mercaptide sulfur donors of the tetradentate L-N_2S_2 chelating ligand, denoted S_{180}, coordinates to molybdenum in the equatorial plane such that the O≡Mo–S_{180}–C_{phenyl} dihedral angle is ∼180°, resulting in a highly covalent π-bonding interaction between an S_{180} p orbital and the molybdenum d_{xy} orbital. This highly covalent bonding scheme is the origin of an intense low-energy S → Mo d_{xy} bonding-to-antibonding LMCT transition (E_{max} ∼16 000 cm^{-1}, ϵ ∼ 4000 M^{-1} cm^{-1}). Spectroscopically calibrated bonding calculations performed at the DFT level of theory reveal that S_{180} contributes ∼22% to the HOMO, which is predominantly a π antibonding molecular orbital between Mo d_{xy} and the S_{180} p orbital oriented in the same plane. The second sulfur donor of the L-N_2S_2 ligand is essentially nonbonding with Mo d_{xy} due to an O≡Mo–S–C_{phenyl} dihedral angle of ∼90°. Because the formal Mo d_{xy} orbital is the electroactive or redox orbital, these Mo d_{xy}–S 3p interactions are important with respect to defining key covalency contributions to the reduction potential in monooxomolybdenum thiolates, including the one- and two-electron reduced forms of sulfite oxidase. Interestingly, the highly covalent Mo–S_{180} π bonding interaction observed in these complexes is analogous to the well-known Cu–S_{Cys} π bond in type 1 blue copper proteins, which display electronic absorption and resonance Raman spectra that are remarkably similar to these monooxomolybdenum thiolate complexes. Finally, the presence of a covalent Mo–S π interaction oriented orthogonal to the MO≡O bond is discussed with respect to electron-transfer regeneration in sulfite oxidase and Mo═$S_{sulfido}$ bonding in xanthine oxidase.

Introduction

Different combinations of cysteine thiolate, ene-1,2-dithiolate, and terminal sulfido donor ligands are coordinated to molybdenum in the active sites of the three distinct families of pyranopterin molybdenum enzymes.[1] The contributions of these sulfur donor ligands to the unique electronic structures of the enzyme active sites define the specific roles of these ligands during catalytic turnover. The diverse class of pyranopterin molybdenum enzymes is routinely subdivided into three families on the basis of sequence homology and geometric structure of the active site: xanthine oxidase (XO); sulfite oxidase (SO); dimethyl sulfoxide reductase.[1] Despite the obvious structural differences, most of the members of these three families catalyze formal oxygen atom transfer (OAT) reactions that are coupled to two-electron redox processes. For example, SO catalyzes the oxidation of sulfite to sulfate and XO catalyzes the hydroxylation of various aromatic heterocycles by formal insertion of an oxygen atom into a C−H bond. Scheme 1 depicts the consensus active site geometries, derived from X-ray crystallography and EXAFS, of XO^{2-10} and SO^{10-15}

* To whom correspondence should be addressed. E-mail: jenemark@u.arizona.edu (J.H.E.); mkirk@unm.edu (M.L.K.).
[†] The University of New Mexico.
[‡] University of Arizona.

(1) Hille, R. *Chem. Rev.* **1996**, *96*, 2757.
(2) Bordas, J.; Bray, R. C.; Garner, C. D.; Gutteridge, S.; Hasnain, S. S. *J. Inorg. Biochem.* **1979**, *11*, 181.
(3) Romao, M. J.; Archer, M.; Moura, I.; Moura, J. J. G.; Legall, J.; Engh, R.; Schneider, M.; Hof, P.; Huber, R. *Science* **1995**, *270*, 1170.
(4) Rebelo, J.; Macieira, S.; Dias, J. M.; Huber, R.; Ascenso, C. S.; Rusnak, F.; Moura, J. J. G.; Moura, I.; Romao, M. J. *J. Mol. Biol.* **2000**, *297*, 135.

10.1021/ic034206n CCC: $27.50
Published on Web 02/06/2004

Scheme 1

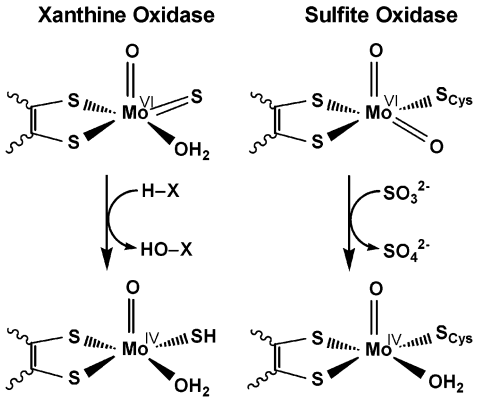

before (oxidized form) and after (reduced form) the OAT half-reaction of the catalytic cycle. The resting state for both families is the oxidized form, $[MoOS]^{2+}$ for XO and $[MoO_2]^{2+}$ for SO, which is converted to a reduced monooxo $[MoO]^{2+}$ site following the substrate oxidation. A monooxomolybdenum active site is hypothesized to be the operative structure for the coupled electron−proton-transfer half-reaction that regenerates the resting state for members of all three enzyme families and completes the catalytic cycle.[16,17] The active site coordination geometry in both the XO and SO families is approximately square pyramidal with two sulfur donors of an ene-1,2-dithiolate from the pyranopterin in the equatorial plane oriented cis to an axial terminal oxo ligand.[18] In addition to the ene-1,2-dithiolate ligation, a terminal sulfido ligand in XO and a cysteine thiolate ligand in SO, both of which are necessary for catalytic activity, are also coordinated in the equatorial plane. The terminal sulfido ligand in XO is protonated upon reduction and the strong coupling of this sulfhydryl proton in EPR spectra suggests that the proton is oriented in the equatorial plane, supporting the notion of an equatorial sulfido ligand in oxidized XO.[19−21] The orientation of the sulfhydryl proton may modulate the

Chart 1

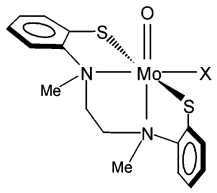

X Substituent	Complex number
Cl	1
$SCH_2–C_6H_5$	2
$SC_6H_4–OCH_3$	3
$SC_6H_4–CF_3$	4

effective orbital overlap between the in-plane molybdenum d_{xy} redox orbital and a sulfhydryl p orbital, affecting electron transfer regeneration of the active site. A coordinated cysteine is conserved throughout all the members of the SO family[22−24] and is required for enzyme function.[25] Furthermore, an A208D human SO mutant is postulated to possess an altered $Mo-S_{Cys}$ coordination geometry that deleteriously affects the enzyme function.[12] This hypothesis is supported by EXAFS spectroscopy of the A208D mutant which indicates a change in the $Mo-S_{Cys}$ bond length compared to that observed for wild-type SO.[26] Spectroscopic studies of small molecules with coordination geometries similar to these pyranopterin molybdenum enzyme active sites, or key components of the active sites, have proven invaluable to the development of active site electronic structure descriptions and proposed roles for individual ligands in facilitating catalysis.[17,27−41] Here we focus on using monooxomolybdenum thiolate complexes as models for the coordinated cysteine in reduced SO and the sulfido/sulfhydryl ligand in XO.

Chart 1 depicts the coordination geometry of the four complexes in this study, *cis*,*trans*-((*N*,*N*′-dimethyl-*N*,*N*′-bis-

(5) Enroth, C.; Eger, B. T.; Okamoto, K.; Nishino, T.; Nishino, T.; Pai, E. F. *Proc. Natl. Acad. Sci. U.S.A.* **2000**, *97*, 10723.
(6) Bordas, J.; Bray, R. C.; Garner, C. D.; Gutteridge, S.; Hasnain, S. S. *Biochem. J.* **1980**, *191*, 499.
(7) Tullius, T. D.; Kurtz, D. M.; Conradson, S. D.; Hodgson, K. O. *J. Am. Chem. Soc.* **1979**, *101*, 2776.
(8) Cramer, S. P.; Hille, R. *J. Am. Chem. Soc.* **1985**, *107*, 8164.
(9) Hille, R.; George, G. N.; Eidsness, M. K.; Cramer, S. P. *Inorg. Chem.* **1989**, *28*, 4018.
(10) Cramer, S. P.; Wahl, R.; Rajagopalan, K. V. *J. Am. Chem. Soc.* **1981**, *103*, 7721.
(11) George, G. N.; Pickering, I. J.; Kisker, C. *Inorg. Chem.* **1999**, *38*, 2539.
(12) Kisker, C.; Schindelin, H.; Pacheco, A.; Wehbi, W. A.; Garrett, R. M.; Rajagopalan, K. V.; Enemark, J. H.; Rees, D. C. *Cell* **1997**, *91*, 973.
(13) George, G. N.; Garrett, R. M.; Prince, R. C.; Rajagopalan, K. V. *J. Am. Chem. Soc.* **1996**, *118*, 8588.
(14) George, G. N.; Kipke, C. A.; Prince, R. C.; Sunde, R. A.; Enemark, J. H.; Cramer, S. P. *Biochemistry* **1989**, *28*, 5075.
(15) George, G. N.; Garrett, R. M.; Graf, T.; Prince, R. C.; Rajagopalan, K. V. *J. Am. Chem. Soc.* **1998**, *120*, 4522.
(16) Jones, R. M.; Inscore, F. E.; Hille, R.; Kirk, M. L. *Inorg. Chem.* **1999**, *38*, 4963.
(17) Inscore, F. E.; McNaughton, R. L.; Westcott, B. L.; Helton, M. E.; Jones, R.; Dhawan, I. K.; Enemark, J. H.; Kirk, M. L. *Inorg. Chem.* **1999**, *38*, 1401.
(18) Our assignment of an axial oxo ligand in oxidized XO derives from our MCD study of the XO "very rapid" intermediate.[16]
(19) Malthouse, J. P. G.; Gutteridge, S.; Bray, R. C. *Biochem. J.* **1980**, *185*, 767.
(20) Gutteridge, S.; Tanner, S. J.; Bray, R. C. *Biochem. J.* **1978**, *175*, 887.
(21) Gutteridge, S.; Tanner, S. J.; Bray, R. C. *Biochem. J.* **1978**, *175*, 869.
(22) Garde, J.; Kinghorn, J. R.; Tomsett, A. B. *J. Biol. Chem.* **1995**, *270*, 6644.
(23) Neame, P. J.; Barber, M. J. *J. Biol. Chem.* **1989**, *264*, 20894.
(24) Barber, M. J.; Neame, P. J. *J. Biol. Chem.* **1990**, *265*, 20912.
(25) Garrett, R. M.; Rajagopalan, K. V. *J. Biol. Chem.* **1996**, *271*, 7387.
(26) George, G. N. Personal communication.
(27) Helton, M. E.; Kirk, M. L. *Inorg. Chem.* **1999**, *38*, 4384.
(28) McNaughton, R. L.; Helton, M. E.; Rubie, N. D.; Kirk, M. L. *Inorg. Chem.* **2000**, *39*, 4386.
(29) McNaughton, R. L.; Tipton, A. A.; Rubie, N. D.; Conry, R. R.; Kirk, M. L. *Inorg. Chem.* **2000**, *39*, 5697.
(30) Helton, M. E.; Gruhn, N. E.; McNaughton, R. L.; Kirk, M. L. *Inorg. Chem.* **2000**, *39*, 2273.
(31) Rubie, N. D.; Peariso, K.; Doonan, C. J.; George, G. N.; Young, C. G.; Kirk, M. L. Manuscript in preparation.
(32) Izumi, Y.; Glaser, T.; Rose, K.; McMaster, J.; Basu, P.; Enemark, J. H.; Hedman, B.; Hodgson, K. O.; Solomon, E. I. *J. Am. Chem. Soc.* **1999**, *121*, 10035.
(33) McMaster, J.; Carducci, M. D.; Yang, Y. S.; Solomon, E. I.; Enemark, J. H. *Inorg. Chem.* **2001**, *40*, 687.
(34) Astashkin, A. V.; Mader, M. L.; Pacheco, A.; Enemark, J. H.; Raitsimring, A. M. *J. Am. Chem. Soc.* **2000**, *122*, 5294.
(35) Mader, M. L.; Carducci, M. D.; Enemark, J. H. *Inorg. Chem.* **2000**, *39*, 525.
(36) Westcott, B. L.; Gruhn, N. E.; Enemark, J. H. *J. Am. Chem. Soc.* **1998**, *120*, 3382.
(37) Dhawan, I. K.; Enemark, J. H. *Inorg. Chem.* **1996**, *35*, 4873.
(38) Carducci, M. D.; Brown, C.; Solomon, E. I.; Enemark, J. H. *J. Am. Chem. Soc.* **1994**, *116*, 11856.
(39) Dhawan, I. K.; Pacheco, A.; Enemark, J. H. *J. Am. Chem. Soc.* **1994**, *116*, 7911.
(40) Backes, G.; Enemark, J. H.; Loehr, T. M. *Inorg. Chem.* **1991**, *30*, 1839.
(41) George, G. N.; Cleland, W. E.; Enemark, J. H.; Smith, B. E.; Kipke, C. A.; Roberts, S. A.; Cramer, S. P. *J. Am. Chem. Soc.* **1990**, *112*, 2541.

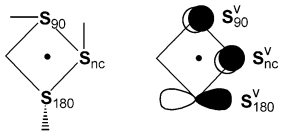

Figure 1. Picture of (L-N_2S_2)MoO(SR) with the view oriented down the Mo≡O bond showing (left) the labeling scheme of the sulfur ligands and orientation of the S−C bond vectors and (right) the orientation of the sulfur 3p orbital (S^v) that is orthogonal to the Mo−S bond.

(2-mercaptophenyl)ethylenediamine)MoO(Cl/SR), which were the first structurally characterized monooxomolybdenum complexes to contain three sulfur donors in the equatorial plane similar to SO and XO.[35,42] These Mo(V) complexes possess a single terminal oxo ligand, a tetradentate ligand (L-N_2S_2) with two sulfur donors and two nitrogen donors, and either a nonchelating thiolate ligand (SR) or a chloride ligand. Detailed EPR and electrochemical studies of the (L-N_2S_2)MoO(SR) series of complexes revealed an electronic ground state that is essentially unaffected by the nature of the nonchelating equatorial ligand.[35] We have performed extensive studies of monooxomolybdenum thiolate complexes which show that the covalency in the Mo−S bond is a function of the O≡Mo−S−C dihedral angle, and these angles can significantly affect the Mo d_{xy}−S p bonding schemes (nonbonding, pseudo-σ bonding, or π bonding) in molecules that have the same first coordination spheres.[29] For clarity, the sulfur 3p orbital that is orthogonal (or vertical) to the Mo−S bond is designated as S^v, the σ-donating sulfur 3p orbital oriented along the Mo−S bond is referred to as S^σ, and the third sulfur 3p orbital is σ-bonded to the carbon. The crystal structures of the (L-N_2S_2)MoO(Cl/SR) complexes[35,43] show that the coordination geometries of the two chelate-constrained sulfur donors of the L-N_2S_2 ligand (Figure 1) are orthogonal to one another; one is oriented such that the O≡Mo−S−C_{phenyl} dihedral angle is ∼90° (S_{90}), and the other is oriented with a O≡Mo−S−C_{phenyl} dihedral angle of ∼180° (S_{180}). The nonchelating sulfur ligands (S_{nc}) in the series all have O≡Mo−S−C dihedral angles of ∼90° in the crystal structures. This coordination geometry orients the S^v_{180} orbital in the equatorial S_3 plane, limiting appreciable orbital interactions to in-plane (orthogonal to the Mo≡O bond) molybdenum d orbitals (Figure 1). Conversely, the S^v_{90} and S^v_{nc} orbitals are orthogonal to the equatorial S_3 plane, restricting orbital interactions to the out-of-plane (parallel with the Mo≡O bond) molybdenum d orbitals. The orientation of the S^v_{90} and S^v_{nc} orbitals of these two cis sulfur atoms is analogous to the out-of-plane orbitals of an ene-1,2-dithiolate ligand.[35] Furthermore, the S^v_{180} interaction with the molybdenum d_{xy} orbital is of a π-type nature.

A biological metal−thiolate π-bonding scheme was first realized in the type 1 blue copper proteins, where it efficiently couples the copper center into a hole superexchange pathway (∼13 Å) for electron transfer that is responsible for oxidation of its redox partner cytochrome b_6f. Whether such a role exists for cysteine in SO remains to be determined; however, the X-ray crystal structure of the (presumably reduced) chicken SO enzyme[12] points toward an S_{90}-type orientation of cysteine relative to Mo≡O that would require reorganization during turnover to form a π bonding interaction with the d_{xy} redox orbital.[29] The XO enzyme family possesses a unique *cis*-MoOS geometry with a very covalent Mo d_{xy}−$S_{sulfido}$ π-type orbital interaction, as indicated by the short Mo═S bond length,[2,6−10] spectroscopic studies of both the enzyme and model complexes, and DFT calculations.[16,31,44,45] For the (L-N_2S_2)MoO(Cl/SR) series investigated here, the structural constraints of the complexes enable the effects of d−p π bonding to be isolated and probed directly. The general implications of these results for biological d−p π bonding schemes in Nature, particularly for metal−sulfur interactions in SO, XO, and blue copper proteins, are also discussed.

Experimental Methods

General Methods and Preparation of Complexes. Complexes **1**−**4** (Chart 1) were synthesized and characterized as previously reported.[35] Spectroscopic samples were prepared in a glovebag under a N_2 stream, and solvents were dried by standard methods to ensure sample integrity.

Electronic Absorption Spectroscopy. Electronic absorption spectra were collected at room temperature on a Hitachi U-3501 UV−vis−NIR spectrophotometer using a double-beam configuration at 2.0 nm resolution. Solution samples were prepared by dissolving the complexes in 1,2-dichloroethane and sealing the sample in 1-cm anaerobic cell with a rubber septum. Solid mull samples were prepared by grinding the solid into a fine powder, dispersing it into poly(dimethylsiloxane), and depositing a thin layer of the mixture between two 1-mm Infrasil quartz disks housed in a custom-designed sample cell.

Magnetic Circular Dichroism (MCD) Spectroscopy. Low-temperature MCD spectra were collected on a system consisting of a Jasco J600 CD spectropolarimeter employing Hamamatsu photomultiplier tubes of either S-1 or S-20 response, an Oxford Instruments SM4000-7T superconducting magnetooptical cryostat (0−7 T, 1.4−300 K), and an ITC503 Oxford Instruments temperature controller. The spectrometer was calibrated for circular dichroism intensity with camphorsulfonic acid, and the wavelength was calibrated using Nd-doped glass. All spectra were collected at 2.0 nm resolution at a temperature of 5 K in an applied magnetic field of 7 T. Samples were prepared by dissolving the complexes in 2:1 2-methyl-THF/DMF and injecting the solution into a ring septum fit between two 1 mm Infrasil quartz disks housed in a custom designed sample cell. Depolarization of the incident radiation by the sample was determined by comparing the intrinsic circular dichroism of a standard Ni (+)-tartrate solution positioned in front of and then in back of each sample.

Resonance Raman (rR) Spectroscopy. Raman spectra were collected in a 135° backscattering geometry using a Coherent Innova (5W) Ar^+ ion laser (457.9−528.7 nm, 9 discrete lines) and a Coherent Innova 300C Kr^+ ion laser (406.7−647.4 nm, 5 discrete lines) as the photon sources. Scattered radiation was dispersed onto a liquid-nitrogen-cooled 1 in. Spex Spectrum One CCD detector

(42) Holm et al. have recently reported a pentacoordinate dioxomolybdenum(VI) complex that contains three sulfur atoms in the equatorial plane: Lim, B. S.; Willer, M. W.; Miao, M.; Holm, R. H. *J. Am. Chem. Soc*. **2001**, *123*, 8343.

(43) Barnard, K. R.; Bruck, M.; Huber, S.; Grittini, C.; Enemark, J. H.; Gable, R. W.; Wedd, A. G. *Inorg. Chem.* **1997**, *36*, 637.

(44) Wilson, G. L.; Greenwood, R. J.; Pilbrow, J. R.; Spence, J. T.; Wedd, A. G. *J. Am. Chem. Soc.* **1991**, *113*, 6803.

(45) George, G. N.; Bray, R. C. *Biochemistry* **1988**, *27*, 3603.

using a Spex 1877E triple grating monochromator equipped with 600, 1200, and 1800 gr/mm holographic gratings at the spectrographic stage. Laser power was kept below 100 mW to prevent possible photo/thermal degradation of the samples. Samples were prepared by dissolving the complexes in benzene or carbon disulfide and sealing the solution in an NMR tube with a rubber septum. The sealed NMR tube was placed into a modified sample holder/spinner for collection of the data. Resonance Raman enhancement profiles were constructed by comparing the integrated intensity of an observed Raman band relative to that of either the 607 cm^{-1} band of benzene or the 655 cm^{-1} band of carbon disulfide. All data were scan averaged, and any individual data set with vibrational bands compromised by cosmic events was discarded.

Electronic Structure Calculations. Density functional theory (DFT) calculations were performed using the Gaussian 98W software[46] package. All calculations employed the B3LYP hybrid functional using a restricted open-shell formalism for Mo(V) models and spin-restricted formalism for Mo(IV/VI) models. A 6-31G basis set was used for all nonmetal atoms, and a polarization function was added to the oxygen and sulfur atoms (6-31G*). The LANL2DZ basis set and LANL2 effective core potentials were used for molybdenum. Computational models substituting NH_3 for amine ligands, H_3CS^- for thiolate ligands, and $(CH_3)_2C_2S_2^{2-}$ for ene-1,2-dithiolate ligands were used. Crystallographic bond lengths, bond angles, and dihedral angles of **1**−**4** were used for the $MoON_2S_3$ and $MoON_2S_2Cl$ cores of the computational models.[35,43] One computational model was used for complexes **2**−**4** using the average crystal structure parameters of the three complexes. The active site of reduced SO was modeled as $[MoO(S_2C_2(CH_3)_2)(SCH_3)(OH_2)]^-$ using the SO crystal structure parameters[12] for the $[MoO(S_2C_2)(SC)O]$ core atoms. The active site of oxidized XO was modeled using $[MoOS(S_2C_2(CH_3)_2)(OH_2)]$ with geometric parameters derived from a combination of crystal structure,[3−5] EXAFS,[2,6−10] and other spectroscopic data.[16,17]

Results and Analysis

Electronic Absorption. Solution electronic absorption spectra of complexes **1**−**4** were collected at room temperature in the 5000−36 400 cm^{-1} energy region, and the data are shown in Figure 2 overlayed with their respective MCD spectra. No low-energy absorptions are observed between 5000 and 11 000 cm^{-1}, and no discernible shoulders are present on the intense absorption feature above 33 000 cm^{-1}. The absorption spectra of all four complexes are remarkably similar, especially in the low-energy region, where an intense ($\epsilon \sim 4000$ M^{-1} cm^{-1}) energetically isolated feature is observed at ~16 000 cm^{-1}. The energy of this broad absorption is characteristic of the $S_{thiolate} \rightarrow$ Mo LMCT transitions observed in numerous monooxo-Mo(V) thiolate complexes.[29,33,47−53] The small shift in energy of the low-energy absorption maxima in the spectra of **1**−**4** ($E_{max} \sim 16$ 000 cm^{-1} for **1,** 15 350 cm^{-1} for **2**, 15 990 cm^{-1} for **3,** 15 450 cm^{-1} for **4**) reflects slight differences in the charge

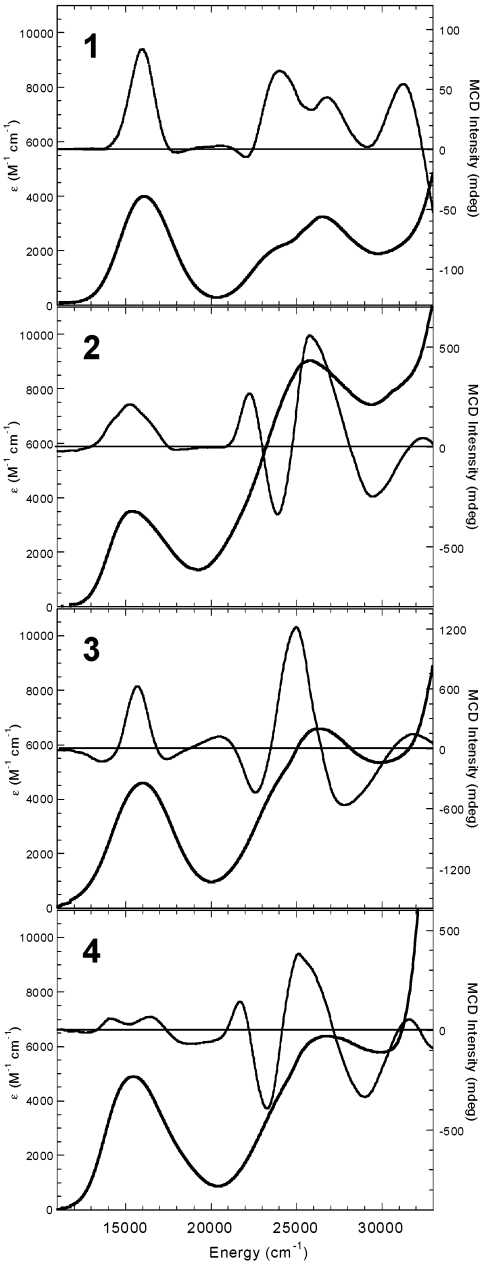

Figure 2. Room-temperature solution electronic absorption (thick line) and 5 K frozen glass MCD (thin line) spectra of (L-N_2S_2)MoOCl (**1**), (L-N_2S_2)MoO($SCH_2C_6H_5$) (**2**), (L-N_2S_2)MoO($SC_6H_4OCH_3$) (**3**), and (L-N_2S_2)MoO($SC_6H_4CF_3$) (**4**).

(46) Frisch, M. J.; Trucks, G. W.; Schlegel, H. B.; Scuseria, G. E.; Robb, M. A.; Cheeseman, J. R.; Zakrzewski, V. G.; Montgomery, J. A., Jr.; Stratmann, R. E.; Burant, J. C.; Dapprich, S.; Millam, J. M.; Daniels, A. D.; Kudin, K. N.; Strain, M. C.; Farkas, O.; Tomasi, J.; Barone, V.; Cossi, M.; Cammi, R.; Mennucci, B.; Pomelli, C.; Adamo, C.; Clifford, S.; Ochterski, J.; Petersson, G. A.; Ayala, P. Y.; Cui, Q.; Morokuma, K.; Malick, D. K.; Rabuck, A. D.; Raghavachari, K.; Foresman, J. B.; Cioslowski, J.; Ortiz, J. V.; Baboul, A. G.; Stefanov, B. B.; Liu, G.; Liashenko, A.; Piskorz, P.; Komaromi, I.; Gomperts, R.; Martin, R. L.; Fox, D. J.; Keith, T.; Al-Laham, M. A.; Peng, C. Y.; Nanayakkara, A.; Gonzalez, C.; Challacombe, M.; Gill, P. M. W.; Johnson, B.; Chen, W.; Wong, M. W.; Andres, J. L.; Gonzalez, C.; Head-Gordon, M.; Replogle, E. S.; Pople, J. A. *Gaussian 98*, revision A.7; Gaussian, Inc.: Pittsburgh, PA, 1998.

(47) Ellis, S. R.; Collison, D.; Garner, C. D. *J. Chem. Soc., Dalton Trans.* **1989**, 413.
(48) Ueyama, N.; Okamura, T. A.; Nakamura, A. *J. Am. Chem. Soc.* **1992**, *114*, 8129.
(49) Boyd, I. W.; Dance, I. G.; Murray, K. S.; Wedd, A. G. *Aust. J. Chem.* **1978**, *31*, 279.
(50) Hanson, G. R.; Brunette, A. A.; McDonell, A. C.; Murray, K. S.; Wedd, A. G. *J. Am. Chem. Soc.* **1981**, *103*, 1953.
(51) Ueyama, N.; Yoshinaga, N.; Kajiwara, A.; Nakamura, A. *Chem. Lett.* **1990**, 1781.
(52) Ueyama, N.; Zaima, H.; Nakamura, A. *Chem. Lett.* **1986**, 1099.
(53) Ueyama, N.; Zaima, H.; Nakamura, A. *Chem. Lett.* **1985**, 1481.

donating ability of the nonchelating ligand. The band shape of this intense low-energy feature in the spectra of **2**−**4** is asymmetrically skewed to the high-energy side of the band, resulting in greater intensity in the trough region at ∼20 000 cm^{-1} when compared to the spectrum of **1**. The general similarity of all four spectra extends into the higher energy region where a broad absorption feature is observed at ∼26 000 cm^{-1}, with a shoulder at ∼23 000 cm^{-1}, followed by additional intense absorption above 30 000 cm^{-1}. Note that the molar extinction coefficient of the ∼26 000 cm^{-1} band of **1** ($\epsilon \sim 3500\ M^{-1}\ cm^{-1}$) is significantly less than those of **2**−**4**, which is likely a result of the additional thiolate ligation in **2**−**4**. Furthermore, the molar extinction coefficient of the high energy band for **2**, which possesses a benzyl mercaptide ligand, is ∼2500 $M^{-1}\ cm^{-1}$ greater than complexes **3** and **4**, which possess phenyl mercaptide ligands ($\epsilon \sim 9000\ M^{-1}\ cm^{-1}$ for **2**, 6700 $M^{-1}\ cm^{-1}$ for **3**, 6400 $M^{-1}\ cm^{-1}$ for **4**). Solid-state absorption spectra of all four complexes also possess a broad absorption band with maxima in the 14 000−16 000 cm^{-1} region, indicating that minimal geometric changes accompany solvation (see Figure S1 in Supporting Information). This is particularly important with respect to the orientation of the sulfur 3p orbital on the nonchelating thiolate ligand (S_{nc}^{v}) in **2**−**4**.

MCD. The 5 K/7 T frozen glass MCD spectra of complexes **1**−**4** were collected between 9500 and 35 000 cm^{-1} and are displayed in Figure 2. The MCD spectrum of **1** clearly appears to violate the MCD "sum rule" as it is dominated by positive C-term features, indicative of excited state-ground state mixing.[54] This differs substantially from the presence of positive and negative features of comparable intensity in the spectra of **2**−**4** and indicates different MCD intensity gaining mechanisms (vide infra) for the transitions of **1** compared to those of **2**−**4**. The same number of spectral transitions are expected for **2**−**4** given that they possess similar coordination geometries and identical first coordination spheres.

The MCD spectrum of **1** displays a symmetric positive C-term band[55] that corresponds to the intense low energy absorption feature at 16 000 cm^{-1}, whereas three C-term bands of varying sign and intensity are observed in this energy region for **2**−**4**. Three positive C-term bands are observed in the spectrum of **2** with maxima at 14 000, 15 500, and 17 000 cm^{-1} and in the spectrum of **4** at 13 900, 15 200, and 16 200 cm^{-1}. Complex **3** possesses a negative−positive−negative C-term pattern with maxima at 13 800, 15 800, and 17 300 cm^{-1}. Similar to the positive C-term band at 16 000 cm^{-1} in the spectrum of **1**, the maximum of each central (second) C-term band in the spectra of **2**−**4** in the low-energy region corresponds to the maximum of the associated intense absorption feature centered at ∼16 000 cm^{-1}. The MCD spectra of all four complexes contain a number of bands between 18 000−21 000 cm^{-1}, a region of very weak intensity in the absorption spectra. Namely, a weak negative feature is observed at ∼18 000 cm^{-1} in the spectra of **1**, **2**, and **4** but is masked in the spectrum of **3** by a larger negative C-term band at ∼17 300 cm^{-1}. A second negative C-term band at ∼20 500 cm^{-1} is observed only in the spectrum of **4**; however, this transition is also anticipated for **2** and **3** but is likely concealed by the more intense positive C-term band at ∼21 500 cm^{-1}. The spectrum of **4** exhibits the greatest number of bands because its intense low-energy features are the most energetically isolated from the intense higher energy features, which allows observation of the weaker bands present in the 18 000−20 000 cm^{-1} region. The high-energy MCD spectrum of **1** displays an asymmetric positive pseudo-A-term (derivative-shaped) band[55] at ∼22 500 cm^{-1} and a positive C-term band with a maximum at ∼27 000 cm^{-1}. The high-energy MCD spectra of **2**−**4** possess a positive C-term band at ∼21 500 cm^{-1} followed by overlapping positive and negative pseudo-A-term bands at ∼ 24 000 cm^{-1} and ∼ 26 500 cm^{-1}, respectively. These overlapping pseudo-A-term bands result in a negative−positive−negative spectral pattern that is similar to the MCD spectra observed in this energy region for monooxo-Mo(V) *mono*dithiolate complexes.[17,38]

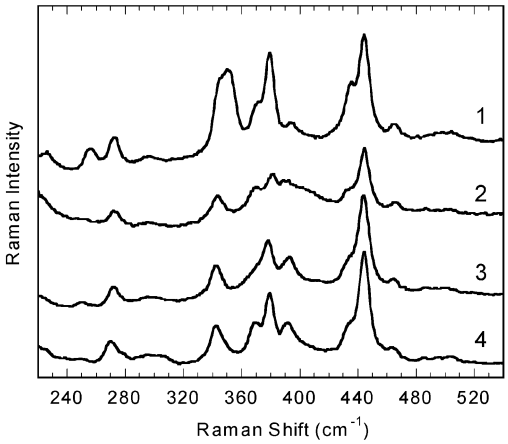

Figure 3. Resonance Raman spectra of (L-N_2S_2)MoOCl (**1**), (L-N_2S_2)-MoO($SCH_2C_6H_5$) (**2**), (L-N_2S_2)MoO($SC_6H_4OCH_3$) (**3**), and (L-N_2S_2)MoO(SC_6H_4-CF_3) (**4**) in benzene at room temperature using 647.1 nm excitation.

Resonance Raman. Solution resonance Raman (rR) spectra of complexes **1**−**4** were collected in benzene and carbon disulfide at room temperature using laser excitation wavelengths between 676.4 and 413.1 nm. The spectra shown in Figure 3 were collected using 647.1 nm (15 454 cm^{-1}) excitation, which is on-resonance with the intense low-energy absorption feature. Typically, less than four rR bands are observed below 600 cm^{-1} for oxomolybdenum thiolate and oxomolybdenum dithiolate complexes,[17,28−29] whereas numerous rR bands are observed below 600 cm^{-1} for **1**−**4**, indicative of a significantly more complex vibrational structure for these complexes. The spectra of **1**−**4** display the same number of vibrational bands between 240 and 520 cm^{-1} (Table 1) with the exception of one additional band at 351 cm^{-1} in the spectrum of **1**. This 351 cm^{-1} band is reasonably attributed to the ν_{Mo-Cl} stretching mode as it is

(54) Neese, F.; Solomon, E. I. *Inorg. Chem.* **1999**, *38*, 1847.
(55) C-term features possess maximum intensity at an energy that directly corresponds to the absorption maximum. Pseudo-A-term features are derivative-shaped with zero intensity at the energy corresponding to the absorption maximum. See: Piepho, S. B.; Schatz, P. N. *Group Theory in Spectroscopy with Applications to Magnetic Circular Dichroism*; Wiley-Interscience: New York, 1983.

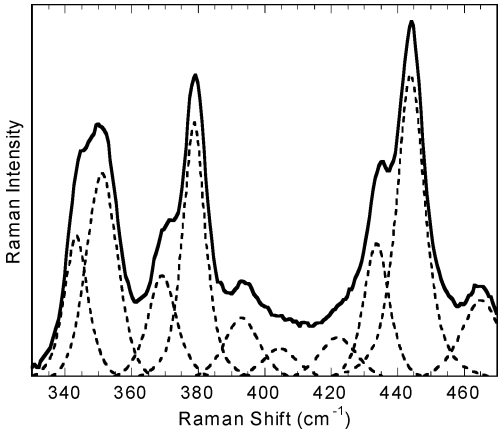

Figure 4. Gaussian-resolved resonance Raman spectrum of (L-N_2S_2)-MoOCl (**1**) in benzene at room temperature using 647.1 nm excitation.

Table 1. Selected Raman Vibrational Frequencies (cm^{-1})

1	2	3	4	tentative assgnt
256	250	250	250	Mo−N_{ax} stretch
274	276	273	271	Mo−N_{eq} stretch
344	345	343	343	
351				Mo−Cl stretch
369	369	368	368	
378	382	378	379	
394	394	393	392	
404	403	404	405	
422	418	417	416	
433	434	434	433	
444	445	444	444	Mo−S_{180} stretch
465	467	466	464	
961	939	937	943	Mo≡O stretch

only observed for **1**,and its energy compares favorably with the totally symmetric 354 cm^{-1} ν_{Mo-Cl} stretch observed in $[MoOCl_4]^-$.[56] Spectral deconvolution of the clustered peaks observed between 330 and 470 cm^{-1} results in 10 bands for **1** (Figure 4) and nine bands for **2**−**4** with nearly identical energies and slightly varying intensities (Figure S2).[57] In all four spectra, the most intense bands are consistently present at ∼345, ∼380, and ∼445 cm^{-1} (Table 1 and Figure 3). Two additional relatively intense vibrational bands are observed in all four spectra at ∼275 and ∼465 cm^{-1}, and regions of weak (and broad) intensity are present at ∼300 and ∼500 cm^{-1}. The spectra do not differ significantly as a function of the substituent X (Chart 1), indicating that these vibrational bands arise solely from Mo−S bond distortions and vibrations associated with the L-N_2S_2 ligand, which has a rigid geometry common to all four complexes.

Interestingly, the rR spectra of **1**−**4** bear a striking similarity to type 1 blue copper proteins which characteristically possess a ∼270 cm^{-1} vibration and a cluster of variably intense modes centered at ∼400 cm^{-1}.[58] The large number of low-frequency fundamentals in blue copper proteins have been interpreted to result from strong mixing between the

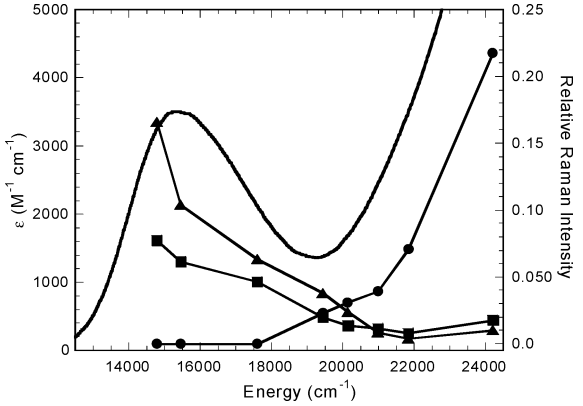

Figure 5. Resonance Raman enhancement profile of the 345 cm^{-1} (squares), 445 cm^{-1} (triangles), and 939 cm^{-1} (circles) bands of (L-N_2S_2)-MoO($SCH_2C_6H_5$) (**2**).

Cu−S_{Cys} stretching mode and internal cysteine ligand coordinates that arises from a coplanar arrangement of the Cu−S−C−C−N portion of the Cu−cysteine framework.[59−64] Similarly for **1**−**4**, the phenyl ring of the S_{180} π-bonding phenylthiolate of the L-N_2S_2 ligand is nearly coplanar with the O≡Mo−S_{180} plane.[35,43] By analogy to the blue copper site, the low-frequency fundamentals observed between 330 and 470 cm^{-1} in the rR spectra of **1**−**4** are reasonably attributable to various kinematically coupled modes of the dominant in-plane Mo−S_{180} stretch with internal modes of the L-N_2S_2 ligand.

The strong intensity of the numerous low-frequency rR vibrational modes in the spectra of **1**−**4** is observed only when using excitation wavelengths greater than 514.5 nm, corresponding to the energy region of the intense low-energy absorption feature. The expected $\nu_{Mo\equiv O}$ stretch at ∼940 cm^{-1} is absent when exciting in this low-energy region. This reveals that the vibrational distortions coupled to the low-energy electronic excitation only involve in-plane Mo−L modes and no distortion of the out-of-plane Mo≡O bond occurs. Higher-energy excitation (λ < 514.5 nm) results in a marked decrease in the intensity of all the low-frequency fundamentals and the emergence of an intense $\nu_{Mo\equiv O}$ stretch, which is indicative of an out-of-plane Mo≡O bond distortion. This extreme orthogonality of enhancement patterns for in-plane and out-of-plane vibrational modes is clearly evident in the rR enhancement profiles of **2** shown in Figure 5. Identical enhancement patterns are observed for **1**, **3**, and **4**. Although the maxima for the 345 and 445 cm^{-1} profiles do not correlate exactly with the absorption maximum, this is

(56) Collin, R. J.; Griffith, W. P.; Pawson, D. *J. Mol. Struct.* **1973**, *19*, 531.
(57) A very weak benzene peak is observed at ∼405 cm^{-1} with off-resonance excitation, but it is believed to be obscured by the resonance enhanced vibrational modes with on-resonance excitation.
(58) Woodruff, W. H.; Dyer, R. B.; Schoonover, J. R. *Resonance Raman Spectroscopy of Blue Copper Proteins*; Biological Applications of Raman Spectroscopy 3; John Wiley & Sons: New York, 1988.
(59) Sanders-Loehr, J. *Investigation of Type I Copper Site Geometry by Spectroscopy and Molecular Redesign*; Bioinorganic Chemistry of Copper; Chapman & Hall: New York, 1993.
(60) Andrew, C. R.; Han, J.; Denblaauwen, T.; Vanpouderoyen, G.; Vijgenboom, E.; Canters, G. W.; Loehr, T. M.; Sanders-Loehr, J. *J. Biol. Inorg. Chem.* **1997**, *2*, 98.
(61) Dong, S. L.; Spiro, T. G. *J. Am. Chem. Soc.* **1998**, *120*, 10434.
(62) Han, J.; Adman, E. T.; Beppu, T.; Codd, R.; Freeman, H. C.; Huq, L.; Loehr, T. M.; Sanders-Loehr, J. *Biochemistry* **1991**, *30*, 10904.
(63) Nestor, L.; Larrabee, J. A.; Woolery, G.; Reinhammar, B.; Spiro, T. G. *Biochemistry* **1984**, *23*, 1084.
(64) Blair, D. F.; Campbell, G. W.; Schoonover, J. R.; Chan, S. I.; Gray, H. B.; Malmstrom, B. G.; Pecht, I.; Swanson, B. I.; Woodruff, W. H.; Cho, W. K.; English, A. M.; Fry, H. A.; Lum, V.; Norton, K. A. *J. Am. Chem. Soc.* **1985**, *107*, 5755.

likely a result of reabsorption (self-absorption) of Raman photons, ligand-field deenhancement, or interference effects caused by another nearby state.[65−71] An overlapping low-energy LMCT or ligand-field state (vide infra) is the probable origin of the observed behavior.

Electronic Structure Calculations. DFT calculations were performed on computational models of **1, 2**−**4**, reduced SO (SO_{red}), and oxidized XO (XO_{ox}). The computational models represent the minimal structural characteristics of the ligands coordinated to molybdenum. Each model geometry contains a single strong-field terminal oxo ligand that dominates the molybdenum ligand field,[72] resulting in a 1−2 eV destabilization of the molybdenum d_{xz} and d_{yz} barycenter relative to the d_{xy} orbital.[17,28,29,33,38] As a result of this energetic isolation, the molybdenum d_{xy} orbital is the only molybdenum d orbital involved in the one-electron redox processes of $d^{0/1/2}$ monooxomolybdenum systems.

The molecular orbital energy diagrams resulting from calculations on $[Mo^{V}O(NH_3)_2(SCH_3)_2Cl]$ and $[Mo^{V}O(NH_3)_2(SCH_3)_3]$, computational models of **1** and **2**−**4**, respectively, are displayed in Figure 6, and the electron density contours and orbital character of the HOMOs (formally the Mo d_{xy} orbitals) are reported in Figure 7 and Table 2, respectively. The low symmetry (C_1) of these structures results in extensive mixing of the atomic orbitals in the calculations; thus, the primary orbital character represented for each molecular orbital in Figure 6 was derived by constructing symmetry adapted linear combinations (SALCs) of ligand p orbitals (separating in-plane and out-of-plane ligand p orbitals) using the calculation results as a guide to the relative energies of the SALCs.

As anticipated, the singly occupied HOMO for calculations of **1** and **2**−**4** (Figure 7a,b) is the formal molybdenum d_{xy} orbital, and its character can be described as a primarily heteronuclear diatomic π-type antibonding interaction between the d_{xy} orbital (∼66%) and the in-plane S^{v}_{180} orbital (∼22%) of the L-N_2S_2 ligand. The S_{90} and S_{nc} atoms of the L-N_2S_2 ligand contribute only ∼2% each to the total orbital character of the HOMO from the $[Mo^{V}O(NH_3)_2(SCH_3)_3]$ calculation. For the $[Mo^{V}O(NH_3)_2(SCH_3)_2Cl]$ calculation, the in-plane Cl p_π orbital (Cl^{π}_{ip}) makes a slightly more significant contribution to the HOMO with ∼6% Cl atomic orbital character, and S_{90} again only contributes 2% to the total orbital character. In both calculations, the S_{90}, S_{nc}, and Cl ligand orbitals covalently mix with d_{xy} at least three times less efficiently than the S^{v}_{180} orbital alone. The strong π-type orbital interaction between d_{xy} and S^{v}_{180} observed in these calculations is analogous to the Cu−S_{Cys} interaction in blue copper proteins, where the Cu $d_{x^2-y^2}$ and S^{v}_{Cys} orbitals form a very covalent π bond.[73]

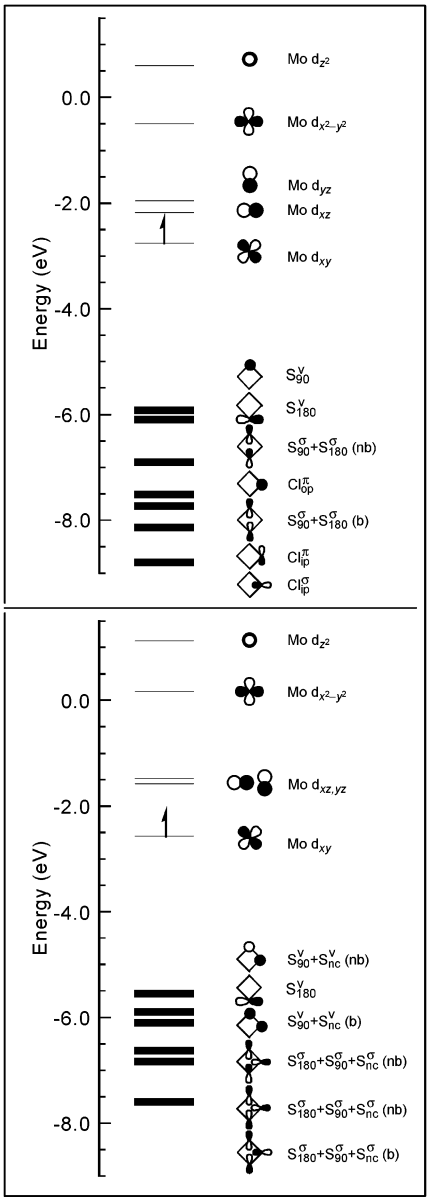

Figure 6. Molecular orbital energy diagrams of ($[MoO(NH_3)_2(SCH_3)_2Cl]$) and ($[MoO(NH_3)_2(SCH_3)_3]$) resulting from DFT calculations. The orbital pictures represent the primary atomic orbital character contributing to each molecular orbital. Orbital energies represented by bold lines are filled, and those represented by thin lines are empty. The view is down the Mo≡O bond, and the equatorial coordinate frame is the same as that shown in Figure 1.

Figure 7c,d displays the molecular orbital contour plots of the Mo d_{xy} HOMO for the reduced SO model ($[Mo^{IV}O(S_2C_2(CH_3)_2)(OH_2)(SCH_3)]^{-}$) with O≡Mo−$S_{thiolate}$−C dihedral angles of 80 and 180°, respectively. This formal Mo d_{xy} orbital is the doubly occupied HOMO in the reduced Mo(IV) state of SO and is singly occupied in the Mo(V) forms of SO that have been extensively studied by EPR.[37,74−76] The HOMO of the reduced SO model with an O≡Mo−$S_{thiolate}$−C

(65) Nafie, L. A.; Pastor, R. W.; Dabrowiak, J. C.; Woodruff, W. H. *J. Am. Chem. Soc.* **1976**, *98*, 8007.
(66) Stein, P.; Miskowski, V.; Woodruff, W. H.; Griffin, J. P.; Werner, K. G.; Gaber, B. P.; Spiro, T. G. *J. Chem. Phys.* **1976**,*64*, 2159.
(67) Bailey, S. E.; Cohan, J. S.; Zink, J. I. *J. Phys. Chem. B* **2000**, *104*, 10743.
(68) Schick, G. A.; Bocian, D. F. *J. Raman Spectrosc.* **1981**, *11*, 27.
(69) Fodor, S. P. A.; Copeland, R. A.; Grygon, C. A.; Spiro, T. G. *J. Am. Chem. Soc.* **1989**, *111*, 5509.
(70) Shin, K. S. K.; Zink, J. I. *J. Am. Chem. Soc.* **1990**, *112*, 7148.
(71) Ribeiro, M. C. C.; Deoliveira, L. F. C.; Constantino, V. R. L.; Toma, H. E.; Santos, P. S. *J. Raman Spectrosc.* **1993**, *24*, 431.
(72) Nugent, W. A.; Mayer, J. M. *Metal-Ligand Multiple Bonds*; Wiley & Sons: New York, 1988.
(73) Solomon, E. I.; Baldwin, M. J.; Lowery, M. D. *Chem. Rev.* **1992**, *92*, 521.

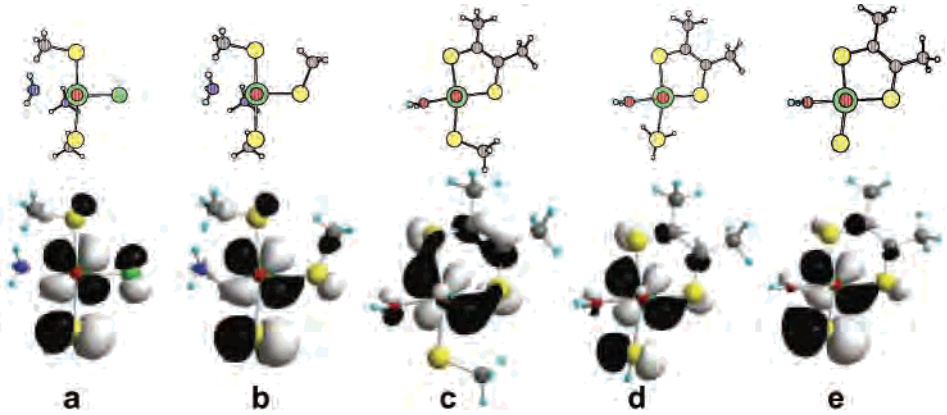

Figure 7. Molecular orbital contour plots of the formal molybdenum d_{xy} orbital of (a) **1**, (b) **2**−**4**, (c) SO_{red} with O≡Mo−S−C angle = 80°, (d) SO_{red} with O≡Mo−S−C angle = 180°, and (e) XO_{ox}.

Table 2. Atomic Orbital Character of the Formal d_{xy} Molecular Orbital (%)

species	computational model	Mo	S_{180}[a]	S_{90}[b]	S[c]	S_{dithio}[d]
1	$Mo^{V}O(NH_3)_2(SCH_3)_2Cl$[e]	66.3	20.2	2.5		
2−**4**	$Mo^{V}O(NH_3)_2(SCH_3)_3$	64.7	23.1	2.2	3.0	
SO_{red}[f]	$[Mo^{IV}O(S_2C_2(CH_3)_2)(OH_2)(SCH_3)]^-$	61.5			1.0	16.0
SO_{red}[g]	$[Mo^{IV}O(S_2C_2(CH_3)_2)(OH_2)(SCH_3)]^-$	61.3			16.8	7.9
XO_{ox}	$Mo^{VI}OS(S_2C_2(CH_3)_2)(OH_2)$	49.1	34.9			4.9

[a] S^{2-} or S with O≡Mo−S−C dihedral angle constrained to ∼180°. [b] S with O≡Mo−S−C dihedral angle constrained to ∼90°. [c] S with O≡Mo−S−C dihedral angle not constrained by chelating. [d] Sum of the two S atoms of a dithiolate chelate. [e] Cl character is ∼6%. [f] SCH_3^- O≡Mo−S−C dihedral angle = 80°. [g] SCH_3^- O≡Mo−S−C dihedral angle = 180°.

dihedral angle of 80° possesses only ∼1% atomic orbital character deriving from the methanethiolate sulfur (Table 2, Figure 7c). This d_{xy}−S^{v} orbital orientation is reminiscent of the d_{xy}−S^{v}_{90} orbital orientation in complexes **1**−**4** and results in essentially no orbital overlap between the thiolate S^{v} and d_{xy} orbitals. Conversely, the HOMO of the reduced SO model with an O≡Mo−$S_{thiolate}$−C dihedral angle of 180° possesses ∼17% atomic orbital character deriving from the methanethiolate sulfur (Table 2, Figure 7d), and the d_{xy}−S^{v} orbital orientation is similar to the π-type interaction of the d_{xy}−S^{v}_{180} orbitals in complexes **1**−**4**. Figure 8 displays the sulfur atomic orbital character in the HOMO, total energies, and Mulliken charge on molybdenum as a function of the O≡Mo−$S_{thiolate}$−C dihedral angle (α) resulting from a series of computations performed on the reduced SO computational model by varying the dihedral angle in 20° increments from 0 to 340°. Changing α from 0/180 to 80° results in a redistribution of the in-plane electron density. This is clearly evident in Figure 7c for α = 80°, where the HOMO possesses very little $S_{thiolate}$ character but substantial $S_{dithiolate}$ character that extends out onto the carbon atoms of the dithiolate ligand. In contrast, as shown in Figure 7d for α = 180°, this HOMO possesses a large degree of $S_{thiolate}$ character and very little $S_{dithiolate}$ character. Qualitatively, the $S_{dithiolate}$ character contributing to the HOMOs reported in Figure 8a is inversely proportional to the $S_{thiolate}$ character over the entire range of angles such that the $S_{thiolate}$ and $S_{dithiolate}$ orbital character is always out-of-phase. The $S_{dithiolate}$ character inthe HOMO at the most energetically stable geometry (α = 80°)

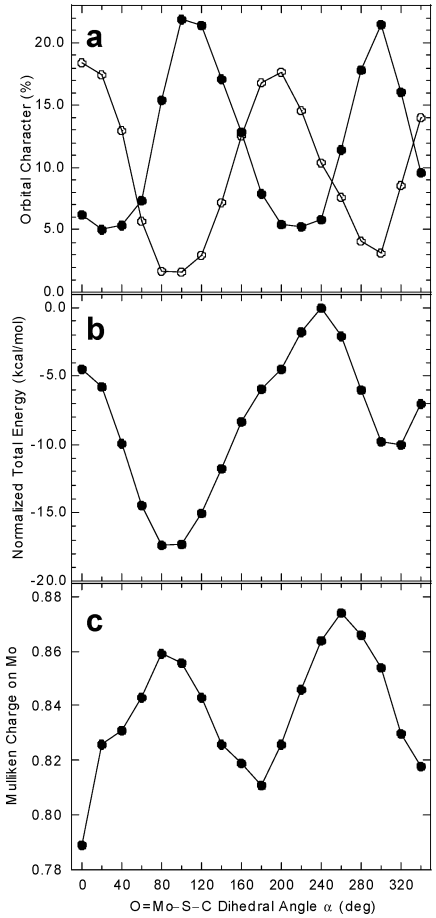

Figure 8. Plots of the O≡Mo−S−C dihedral angle (α) (a) versus $S_{thiolate}$ (open circles) and $S_{dithiolate}$ (closed circles) orbital character and (b) versus total energy, and (c) Mulliken charge on Mo, resulting from a series of DFT calculations on $[MoO(S_2C_2Me_2)(OH_2)(SCH_3)]^-$, a model for SO_{red}.

(74) Hawkes, T. R.; Bray, R. C. *Biochem. J.* **1984**, *222*, 587.
(75) Bray, R. C.; Gutteridge, S.; Lamy, M. T.; Wilkinson, T. *Biochem. J.* **1983**, *211*, 227.
(76) Lamy, M. T.; Gutteridge, S.; Bray, R. C. *Biochem. J.* **1980**, *185*, 397.

is ∼16%. This is a significant contribution to the redox orbital whereas the $S_{thiolate}$ contribution to the HOMO is only ∼2% at this geometry. The dihedral angle range of 40−160°, which is ±60° from where the $S_{dithiolate}$ orbital character is at a maximum, shows a large variation in the $S_{thiolate}$ and $S_{dithiolate}$ orbital character that contributes to the HOMO. The most stable geometry occurs when α is 80°, nearest to the 83.7° angle observed in the crystal structure of SO,[12] and the least stable geometry occurs at α = 240° (Figure 8b). The calculated total energy difference between the most stable and least stable geometries is 17.4 kcal mol^{-1} (0.754 eV), but the maximum energy difference in the 40−160° range is only ∼9 kcal mol^{-1} (0.4 eV). Figure 8c shows that the Mulliken charge on molybdenum increases when α is near 90 and 270° and is reduced when α is 0 and 180°.

Figure 7e shows the contour plot for the analogous orbital of [$Mo^{VI}OS(S_2C_2(CH_3)_2)(OH_2)$], the computational model for oxidized XO. This orbital is the LUMO, unoccupied in the Mo(VI) state of XO, and is singly occupied in the Mo(V) "very rapid" intermediate of XO that has been studied by EPR and MCD.[16,19,44,45,77−81] The extreme inequality of Mo−S covalency among different sulfur donor ligands contributing to the calculated total molecular orbital character of the redox orbital found for complexes **1**−**4** also exists for [$Mo^{VI}OS(S_2C_2(CH_3)_2)(OH_2)$]. In this case, the Mo d_{xy} character is 49.1%, the $S_{sulfido}$ character is 34.9%, and the primary orbital interaction is π-type antibonding between d_{xy} and the in-plane sulfido S^v orbital. This agrees remarkably well with the 38% sulfido contribution to the d_{xy} orbital determined by EPR spectroscopy for the "very rapid" Mo(V) form of XO.[45] The ∼5% contribution from the two dithiolate sulfur atoms is seven times less than that of the terminal sulfido donor. The orientation of the sulfido S^v orbital that overlaps with d_{xy} is the same whether the ligand is a terminal sulfido ligand or thiolate ligand with an O≡Mo−S−C dihedral angle of 180 or 0°. This bonding scheme is nearly identical to the 42% Cu $d_{x^2-y^2}$ and 36% S_{Cys} atomic orbital character determined for the HOMO of blue copper proteins.[73]

Monooxomolybdenum−Thiolate Bonding. The characteristic molybdenum d orbital splitting for typical monooxomolybdenum complexes results from the very strong σ- and π-donor character of the single terminal oxo ligand. This interaction destabilizes the molybdenum d_{z^2} (σ), d_{xz} (π), and d_{yz} (π) orbitals relative to an O_h ligand field.[72] In contrast, the $d_{x^2-y^2}$ orbital, and to a considerably lesser extent the d_{xy} orbital, is destabilized by the equatorial ligands. Therefore, the formal molybdenum d_{xy} orbital is the lowest energy metal orbital with Δt_{2g} ∼13 000−16 000 cm^{-1},[38,72,82,83] making this orbital the redox orbital for high-valent oxo-Mo(IV/V/VI) systems. Thus, the lowest energy charge-transfer bands are expected to be L → Mo d_{xy} ligand-to-metal charge-transfer transitions, and the transitions ∼15 000 cm^{-1} higher in energy are expected to be L → $d_{xz,yz}$ charge-transfer transitions. This has been proven by rR enhancement profiles on (L-N_3)Mo(V)O(dithiolate) complexes in which in-plane ν_{Mo-S} modes were enhanced for in-plane S → d_{xy} excitations and $\nu_{Mo\equiv O}$ modes were enhanced for out-of-plane S → $d_{xz,yz}$ excitations.[17] This orthogonal vibrational mode enhancement provides a direct probe of Mo−S bonding in monooxomolybdenum thiolate complexes.

The ultimate arbiter of covalency between molybdenum d orbitals and monothiolate orbitals in monooxomolybdenum thiolate complexes is the O≡Mo−S−C dihedral angle (α).[29] The amount of S^σ overlap with $d_{x^2-y^2}$ is relatively constant, but large anisotropic covalency can occur as a result of the dependence of $\langle S^v|d_{xy}\rangle$ on α. The S^v orbital is oriented for maximal overlap with d_{xy} when α = 0 or 180°, resulting in a strong π-type orbital interaction. Conversely, when α = 90° the S^v orbital is orthogonal to d_{xy} and $\langle S^v|d_{xy}\rangle = 0$.[84] This variable S^v-d_{xy} overlap directly affects the energy of the redox orbital as well as the effective nuclear charge of the metal and can therefore act to fine-tune the reduction potential of the molybdenum center.[85]

Gaussian Resolution and Band Assignments. Deconvolution of the MCD and electronic absorption spectra, coupled with the rR enhancement profiles, allows for detailed band assignments to be made below 30 000 cm^{-1} for complexes **1**−**4**. These spectral assignments are then used to evaluate the results of bonding calculations. Figure 9 displays the Gaussian resolved MCD and absorption spectra of **1** and **4**, and the assignments given for each band relate to the primary character of the two molecular orbitals involved in the one-electron promotions associated with the electronic transition. The Gaussian-resolved MCD and absorption spectra of **2** and **3** are analogous to **4** and are available in Supporting Information (Figures S3 and S4).

(L-N_2S_2)MoOCl (1). **(a) Band 1.** Band 1 is a weak LMCT transition assigned as S^v_{180} → d_{xy}, an out-of-plane to in-plane transition made allowed by low-symmetry mixing of the S^v_{90} and S^v_{180} orbitals of the L-N_2S_2 ligand. The weak intensity of the transition is a reflection of the small degree of $S^v_{180}-S^v_{90}$ mixing. This mixing is supported by the DFT calculations (∼2% S_{90} orbital character in the HOMO of [$Mo^VO(NH_3)_2(SCH_3)_2Cl$]; see Table 2 and Figure 7a) and is also observed for **2**−**4**.

(b) Band 2. The overwhelming majority of the absorption intensity in this energy region is due to band 2 at 16 000 cm^{-1}. The energies of $S_{thiolate}$ → d_{xy} LMCT transitions in monooxomolybdenum complexes (those that are not perturbed by H-bonding to the thiolate) are consistently observed at ∼16 000 cm^{-1}.[29,33,47−53] Therefore, this transition is assigned as a S^v_{180}→ d_{xy} bonding-to-antibonding LMCT transition. Additional support for this assignment is given by rR

(77) Bray, R. C.; Lowe, D. J. *Biochem. Soc. Trans.* **1997**, *25*, 762.
(78) Greenwood, R. J.; Wilson, G. L.; Pilbrow, J. R.; Wedd, A. G. *J. Am. Chem. Soc.* **1993**, *115*, 5385.
(79) Hille, R.; Kim, J. H.; Hemann, C. *Biochemistry* **1993**, *32*, 3973.
(80) Kim, J. H.; Hille, R. *J. Biol. Chem.* **1993**, *268*, 44.
(81) Manikandan, P.; Choi, E. Y.; Hille, R.; Hoffman, B. M. *J. Am. Chem. Soc.* **2001**, *123*, 2658.
(82) Lever, A. B. P. *Inorganic Electronic Spectroscopy*; Elsevier Science Publishing: New York, 1986.
(83) Sabel, D. M.; Gewirth, A. A. *Inorg. Chem.* **1994**, *33*, 148.
(84) Helton, M. E.; Kirk, M. L. Manuscript in preparation.
(85) Holm, R. H.; Kennepohl, P.; Solomon, E. I. *Chem. Rev.* **1996**, *96*, 2239.

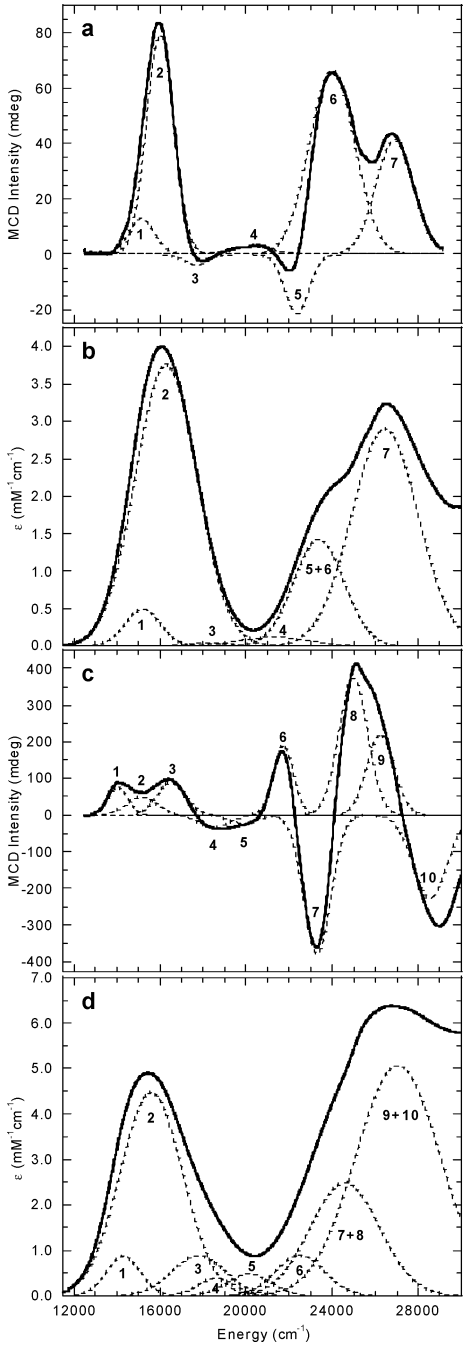

Figure 9. Gaussian-resolved spectra of the (a) MCD of **1**, (b) electronic absorption of **1**, (c) MCD of **4**, and (d) electronic absorption of **4**. The dashed lines are the individual Gaussian bands used in the fit of the data (solid line).

spectroscopy. Laser excitation into this band results in the enhancement of numerous low-frequency vibrational bands that are attributed to various mixed vibrational modes of the $Mo-S_{180}$ stretch and kinematically coupled vibrational modes of the L-N_2S_2 ligand phenyl ring. The d_{xy} orbital is expected to possess significant chloride character derived from π-type overlap with Cl^{π}_{ip}. This is observed in the electron density contour of the HOMO, which shows an ~6% contribution to d_{xy} from the chloride ligand. The energy of this transition would be expected to shift to lower energy if there was appreciable mixing of S^{v}_{180} and Cl^{π}_{ip}, but this is not observed.

Therefore, the difference in valence ionization energies of the phenyl mercaptide sulfur and chloride atomic orbitals leads to relatively inefficient mixing of the S^{v}_{180} and Cl^{π}_{ip} in-plane orbitals with $\langle S^{v}_{180}|d_{xy}\rangle$ greater than $\langle Cl^{\pi}_{ip}|d_{xy}\rangle$.

(c) Band 3. Band 3 is a weak MCD C-term band at 18 000 cm^{-1} that is consistent with assignment as a $d_{xy} \rightarrow d_{x^2-y^2}$ ligand-field transition because the energy of this band is higher than the characteristic $d_{xy} \rightarrow d_{xz,yz}$ ligand-field transition observed for monooxomolybdenum complexes.[38,82,83] A ligand-field transition from d_{xy} to the degenerate $d_{xz,yz}$ set would give rise to a weak MCD pseudo-A band at 13 000−16 000 cm^{-1},[38,83,84,86] and while this transition is expected to occur, it is most likely obscured under band 2. A weak negative MCD C-term band is also observed in **2**−**4** (band 4) at similar energies (vide supra).

(d) Band 4. Band 4 at 21 000 cm^{-1} is assigned as $S^{\sigma}_{90} \rightarrow d_{xy}$ on the basis of its energy and weak intensity. In comparison, the $S^{\sigma} \rightarrow d_{xy}$ LMCT transition of $[MoO(phenylthiolate)_4]^-$ is observed at ~22 000 cm^{-1} with a molar extinction coefficient per sulfur of only ~150 M^{-1} cm^{-1}.[29] The weak intensity of these transitions is attributable to poor $S^{\sigma}_{90}-d_{xy}$ orbital overlap. DFT calculations of both $[MoO(SCH_3)_4]^-$ and $[MoO(NH_3)_2(SCH_3)_2Cl]$ indicate that a slight in-plane rotation of the d_{xy} orbital, a result of low-symmetry mixing with $d_{x^2-y^2}$, is the intensity gaining mechanism for this transition.

(e) Bands 5 and 6. These bands form an asymmetric MCD pseudo-A-term feature that is attributed to a $S^{v}_{90} \rightarrow d_{xz,yz}$ transition. The asymmetry is not unexpected in this low symmetry complex and could result from better overlap of S^{v}_{90} with one of the nearly degenerate $d_{xz,yz}$ orbitals. This is also suggested by the absorption intensity which is weaker than anticipated for a $S \rightarrow d_{xz,yz}$ transition in a monooxomolybdenum thiolate complex. Further support for the spectral assignment is given by the rR enhancement profiles which show large enhancement of $\nu_{Mo\equiv O}$ modes compared to ν_{Mo-S} modes in this energy region. This is direct evidence that the transition involves the Mo≡O π^* orbitals and that the charge transfer donor orbital is not strongly coupled to in-plane molybdenum orbitals.

(f) Band 7. The energy of band 7 is consistent with that observed for $Cl \rightarrow d_{xy}$ LMCT transitions (26 000−30 000 cm^{-1}) in $[Mo(V)OCl_x]^n$ complexes[38,83,86] and is assigned as $Cl^{\pi}_{ip} \rightarrow d_{xy}$. It is a positive MCD C-term band, which indicates involvement of a nondegenerate d orbital, and the large intensity ($\epsilon \approx 3000$ M^{-1} cm^{-1}) of the corresponding absorption band indicates that the transition is a LMCT transition from a covalent ligand orbital. The DFT calculation of $[MoO(NH_3)_2(SCH_3)_2Cl]$ suggests $Cl^{\pi}_{ip}-d_{xy}$ covalency with ~6% chloride character mixed into the molybdenum d_{xy} orbital.

L-N_2S_2MoO−SR (2−4). Given the similar geometric structures of **2**−**4**, the same number of transitions are expected in their spectra. Hence, the same number of Gaussian bands were used for each fitting process, and the energies

(86) Helton, M. E.; Kirk, M. L. Unpublished spectroscopic results on (L-N_3)$Mo^{V}OCl_2$.

and relative intensities of the bands are consistent throughout this series of complexes.

(a) Bands 1−3. These bands in the MCD spectra correspond to the energy region of the intense low-energy absorption feature. Resonance Raman profiles show large enhancement of vibrational bands involving in-plane ν_{Mo-S} modes with excitation in this energy region. Like band 2 of complex **1**, the $S^{v}_{180}-d_{xy}$ π-type orbital overlap dominates the bonding scheme of the ligands with the in-plane Mo d_{xy} orbital and therefore must also dominate the absorption intensity resulting from LMCT transitions to the Mo d_{xy} orbital. Unlike complex **1**, there are *two* other sulfur orbitals (S^{v}_{90} and S^{v}_{nc}) that are expected to be orthogonal to d_{xy}, indicated by the O≡Mo−S−C dihedral angles of ∼90° observed in the crystal structures of **2**−**4**, and these can mix to form in-phase and out-of-phase linear combinations. One combination will be nonbonding with respect to $d_{xz,yz}$ ([S^{v}_{90} + S^{v}_{nc}(nb)]), and the other will be bonding with $d_{xz,yz}$ ([S^{v}_{90} + S^{v}_{nc}(b)]). Thus, a total of three low-energy LMCT transitions to d_{xy} are possible due to mixing of S^{v}_{180}, [S^{v}_{90} + S^{v}_{nc}(nb)], and [S^{v}_{90} + S^{v}_{nc}(b)] as a result of low symmetry. This allows for the assignment of band 1 as [S^{v}_{90} + S^{v}_{nc}(nb)] → d_{xy}, band 2 as S^{v}_{180} → d_{xy}, and band 3 as [S^{v}_{90} + S^{v}_{nc}(b)] → d_{xy}. The S^{v}_{180} → d_{xy} transition is assigned as band 2 because this band dominates the intensity of the low-energy absorption feature in all three complexes and derives its intensity from the strong $S^{v}_{180}-d_{xy}$ π-type orbital overlap. The absorption intensity of bands 1 and 3 relative to band 2 is proportional to the amount of S^{v}_{180} orbital character covalently mixed into the [S^{v}_{90} + S^{v}_{nc} (nb)] and [S^{v}_{90} + S^{v}_{nc}(b)] molecular orbitals. Finally, the variation in sign of the three MCD bands in **2**−**4** very likely reflects differences in the magnitude of out-of-state spin−orbit coupling matrix elements between these three charge-transfer excited-state configurations that result from thiolate → Mo one-electron promotions.[54] The precise origin of these differences is difficult to ascertain due to the low symmetry of the complexes and is beyond the scope of this work.

(b) Band 4. Band 4 is a weak negative MCD C-term band that is revealed most prominently in the MCD spectra of **2** and **4** because bands 1−3 occur at lower energies for these complexes than for **3**. The transition energy and weak absorption intensity of this band allow for its assignment as a d_{xy} → $d_{x^2-y^2}$ ligand-field transition (compare to band 3 of **1**).

(c) Bands 5 and 6. These bands are assigned as S^{σ}(nb) → d_{xy} LMCT transitions. Their weak absorption intensity results from poor overlap between the two nonbonding SALCs of S^{σ} orbitals and the d_{xy} orbital. The energy and intensity of these bands compare well with the S^{σ}(nb) → d_{xy} LMCT transition of [MoO(phenylthiolate)$_4$]$^-$ as well as band 4 of complex **1**.[29] Low-symmetry $d_{xy}-d_{x^2-y^2}$ mixing is the intensity gaining mechanism for these weak transitions.

(d) Bands 7 and 8. These transitions display a positive MCD pseudo-A feature centered at ∼24 000 cm^{-1}, which corresponds to the prominent shoulder on the low-energy side of the ∼28 000 cm^{-1} absorption feature. These bands are assigned as out-of-plane to out-of-plane [S^{v}_{90} + S^{v}_{nc}(nb)] → $d_{xz,yz}$ LMCT transitions. The fact that these are MCD pseudo-A terms and that large rR enhancement of the $\nu_{Mo\equiv O}$ mode occurs with excitation in this region provide evidence that these transitions involve the degenerate d_{xz} and d_{yz} Mo≡O π^* orbitals.[17]

(e) Bands 9 and 10. These transitions result in a negative MCD pseudo-A feature at ∼28 000 cm^{-1} and are similar to bands 7 and 8 with the exception of the sign of the MCD feature. These bands are assigned as bonding-to-antibonding [S^{v}_{90} + S^{v}_{nc}(b)] → $d_{xz,yz}$ LMCT transitions. They originate from the same set of S^{v} orbitals as bands 7 and 8, but the bonding-to-antibonding transition is expected to occur at higher energy, possess greater absorption intensity, and display greater $\nu_{Mo\equiv O}$ enhancement in the rR profiles. Further support for this assignment and the assignment of bands 7 and 8 derives from comparison to (L-N_3)Mo(V)O(dithiolate) complexes, which have the same orbital orientation of the out-of-plane sulfur 3p orbitals of the dithiolate relative to d_{xz} and d_{yz}. These complexes display out-of-plane S → $d_{xz,yz}$ LMCT transitions at ∼22 000 cm^{-1} ($\epsilon \approx 1100$ M^{-1} cm^{-1}) and ∼25 000 cm^{-1} ($\epsilon \approx 5500$ M^{-1} cm^{-1}).[17,38]

Discussion

The principal contributor to the intense low-energy absorption feature observed for complexes **1**−**4** is a S^{v}_{180} → d_{xy} LMCT transition resulting from a strong π-bonding interaction between the S^{v}_{180} and molybdenum d_{xy} orbitals. Complexes **2**−**4** possess two additional very weak charge-transfer bands that also contribute to the broad absorption envelope. These weak bands gain intensity by mixing with the intense S^{v}_{180} → d_{xy} π-type bonding-to-antibonding LMCT transition, and the oscillator strength ratios of these bands are proportional to the percentage of S^{v}_{180} orbital character mixed into these two other sulfur donor orbitals (S^{v}_{90} and S^{v}_{nc}). Resonance Raman excitation profiles of **1**−**4** display a remarkable orthogonal enhancement of in-plane ν_{Mo-S} modes versus out-of-plane $\nu_{Mo\equiv O}$ modes. Strong resonance enhancement of $\nu_{Mo-S_{180}}$ occurs with excitation under the low-energy absorption envelope without the observation of $\nu_{Mo\equiv O}$ resonance enhancement. Thus, the rR data are consistent with the assignment of the low-energy absorption feature as a S^{v}_{180} → d_{xy} LMCT transition.[17] Electronic structure calculations provide additional insight into the bonding schemes of **1**−**4**. The HOMOs are essentially heteronuclear diatomic with ∼60% molybdenum d_{xy} and ∼22% S^{v}_{180} orbital character arising from a covalent $S^{v}_{180}-d_{xy}$ π-bonding interaction (Figure 7a,b). The higher energy (>18 000 cm^{-1}) MCD bands of **2**−**4** are strikingly similar to those of (L-N_3)Mo^{V}O-(dithiolate) complexes[17,38] and the "very rapid" intermediate of XO.[16] Thus, this region of the MCD spectrum provides a spectroscopic signature for two cis sulfur donors with S^{v} orbitals oriented parallel to a terminal oxo ligand (S^{v}_{90} and S^{v}_{nc} of Figure 1).

Similarities to Cu−S_{Cys} Bonding in Blue Copper Proteins. The energy and intensity of the low-energy absorption band in complexes **1**−**4** compare remarkably well

to the characteristic $S_{Cys} \rightarrow Cu\ d_{x^2-y^2}$ LMCT transition observed for blue copper proteins ($E_{max} \approx 16\ 000\ cm^{-1}$, $\epsilon \sim 5000\ M^{-1}\ cm^{-1}$).[73] This spectral resemblance is the result of an equivalent metal−thiolate bonding scheme that arises from similar orientation of the S^v thiolate orbital relative to the in-plane metal redox orbital (Mo−S_{180}[35,43] and Cu−S_{Cys}[73]). This 180° orientation is defined by the O≡Mo−S_{180}−C dihedral angle in **1**−**4** and the 0° S_{Met}−Cu−S_{Cys}−C_β dihedral angle in blue copper proteins. These second coordination sphere effects result in a strong in-plane S^v−d π-type interaction for both systems, with the HOMOs of each being effectively described as heteronuclear diatomic M−S π antibonding. The similarities of these monooxomolybdenum thiolate complexes to blue copper proteins extends beyond their geometric structures and electronic absorption spectra to include their resonance Raman vibrational spectra as well.[58,59] At least nine low-frequency fundamentals are observed between 220 and 480 cm^{-1} in **1**−**4** and *poplar* plastocyanin when exciting into the intense low energy absorption envelope.[61] Several studies involving isotopic substitution of the coordinated cysteine (^{34}S, ^{15}N-Cys, β-D_2-Cys) in plastocyanin and azurin show isotopic shifts of these low-frequency fundamentals, providing evidence for extensive kinematic coupling between the Cu−S_{Cys} stretch and internal ligand modes.[60−64] Furthermore, the ligand modes that are kinematically coupled to the dominant Cu−S_{Cys} stretch and are resonantly enhanced involve bonds that are coplanar with either the Cu−S_{Cys} or Cu−N_{His} bond vector, namely, $C_\beta C_\alpha N$ of cysteine and the imidazole ring of one of the coordinated histidines.[61,62] Likewise, the crystal structures of **1**−**4** reveal that the phenyl carbon atoms of the S_{180} phenyl mercaptide are coplanar with the Mo−S_{180} bond vector and that the axial nitrogen atom, ethane carbon atoms, and methyl carbon atoms (of the L-N_2S_2 ligand) are coplanar with the Mo−$N_{equatorial}$ bond vector.[35] Small molecule model complexes of the blue copper active site have been synthesized, and although their electronic absorption spectra are quite similar to that of the proteins, their rR spectra do not display the complexity found for blue copper spectra or the complexes presented here.[87,88] The thiolate ligands in these blue copper models have been designed to be sterically constrained by incorporation of large ancillary groups to ensure good orbital overlap between the thiolate S^v and Cu $d_{x^2-y^2}$ orbitals. However, the ligand architecture is not constrained as part of a chelate ring, as is the case for complexes **1**−**4** in this study. Interestingly, the rigidity of the L-N_2S_2 ligand in **1**−**4** appears to provide a very good model for the torsionally constrained protein backbone of the copper-bound S_{Cys}, resulting in complex rR spectra that closely resemble the blue copper spectra. Analysis of the vibrational modes of **1**−**4** is currently underway in our laboratory.

Implications for ET in SO. The highly covalent Cu−S_{Cys} π-bonding interaction in *poplar* plastocyanin enhances the electronic coupling factor for long-range electron transfer between the copper center and a solvent-exposed tyrosine side chain in the reduction of plastocyanin by cytochrome b_6f.[61,89,90] Thus, the question arises as to whether the coordinated cysteine in reduced SO similarly couples the molybdenum active site to long-range hole superexchange pathways for electron-transfer regeneration of the oxidized active site. The oxidized active site of vertebrate SO is regenerated following oxygen atom transfer via two sequential one-electron transfers from the molybdenum active site to an endogenous b heme located in a separate domain. The molybdenum and heme domains are connected to each other by a single polypeptide loop,[12] and it has been proposed that the b heme propionate groups electrostatically interact with a positive patch on the molybdenum domain at or near the substrate access channel.[91] Because the coordinated S_{Cys} is oriented in the direction of this channel, there is the implication that S_{Cys} may play a key role in the electron transfer regeneration process. As in the case of blue copper proteins, this would likely be facilitated by a covalent Mo−S_{Cys} π-bonding interaction. However, X-ray crystallography on a reduced form of chicken SO[12] indicates that the O≡Mo−S_{Cys}−C dihedral angle is ∼84°, and this is supported by an MCD study of a paramagnetic Mo(V) form of chicken SO.[92] This geometry is in agreement with the results of our DFT calculations on the reduced SO active site where O≡Mo−S_{Cys}−C dihedral angles in the range of 80−100° resulted in the lowest total energies (Figure 8b), and the $S_{dithiolate}$−Mo d_{xy} orbital overlap is substantially greater than the $S_{thiolate}$−Mo d_{xy} overlap at this geometry. This also supports prior studies which suggested that electron transfer occurs via a σ-mediated pathway involving the in-plane sulfur orbitals of the pyranopterin-ene-1,2-dithiolate.[16,17] However, it is possible that the O≡Mo−S_{Cys}−C dihedral angle is dynamic during the course of catalysis, enabling the molybdenum active site to couple into hole superexchange pathways for electron transfer using cysteine in a manner analogous to the blue copper proteins. Our DFT results show that the cysteine sulfur contributes ∼18% to the total orbital character of the reduced SO HOMO when the O≡Mo−S_{Cys}−C dihedral angle is either 0 or 180°, which is substantially greater than the ∼7% contribution of the ene-1,2-dithiolate sulfurs at this geometry. Further, the bonding calculations clearly show that an inverse relationship exists between the orbital character contribution to the HOMO of the cysteine thiolate and ene-1,2-dithiolate as the O≡Mo−S_{Cys}−C dihedral angle is varied (Figure 8a). Alternatively, changes in the O≡Mo−S_{Cys}−C dihedral angle could simply serve to modulate the covalency of the ene-1,2-dithiolate sulfur donors of the pyranopterin, indirectly affecting the energy of the redox orbital and facilitating the oxygen atom transfer and electron-transfer half-reactions. This is a viable

(87) Randall, D. W.; George, S. D.; Hedman, B.; Hodgson, K. O.; Fujisawa, K.; Solomon, E. I. *J. Am. Chem. Soc.* **2000**, *122*, 11620.
(88) Randall, D. W.; George, S. D.; Holland, P. L.; Hedman, B.; Hodgson, K. O.; Tolman, W. B.; Solomon, E. I. *J. Am. Chem. Soc.* **2000**, *122*, 11632.
(89) Beratan, D. N.; Betts, J. N.; Onuchic, J. N. *Science* **1991**, *252*, 1285.
(90) Lowery, M. D.; Guckert, J. A.; Gebhard, M. S.; Solomon, E. I. *J. Am. Chem. Soc.* **1993**, *115*, 3012.
(91) Pacheco, A.; Hazzard, J. T.; Tollin, G.; Enemark, J. H. *J. Biol. Inorg. Chem.* **1999**, *4*, 390.
(92) Helton, M. E.; Pacheco, A.; McMaster, J.; Enemark, J. H.; Kirk, M. L. *J. Inorg. Biochem.* **2000**, *80*, 227.

possibility given the known versatile charge donating ability of ene-1,2-dithiolate ligands[17,27,30,36,93,94] and the modulation of the charge on molybdenum as a function of the O≡Mo−S−C torsion angle (Figure 8c). Detailed spectroscopic and electronic structure studies of structurally characterized monooxomolybdenum model complexes that incorporate both ene-1,2-dithiolate and thiolate ligands are needed to thoroughly evaluate the covalency contributions of these ligands to the oxygen atom transfer and electron-transfer processes in SO.[42,95]

Molybdenum−Sulfido Bond in XO. Spectroscopic studies on XO and [(L-N_3)MoOS(OPh)]$^{5/6+}$ model complexes, coupled with detailed electronic structure calculations, provide compelling evidence for a heteronuclear diatomic Mo−S π-bonding scheme in the "very rapid" and oxidized forms of XO.[31,44,45,78] The electron density contour of the oxidized XO LUMO in Figure 7e illustrates this description and shows that the in-plane S^{π} orbital orientation of the terminal sulfido ligand is the same as that of the S^{v}_{180} orbital in complexes **1**−**4**.[96] However, in stark contrast to **1**−**4** and blue copper proteins, a low-energy $S^{\pi}_{sulfido} \rightarrow$ Mo LMCT transition is not observed for oxidized XO[97] or [MoOS]$^{2+}$ model complexes.[31,98] This reflects key differences in the strength of the Mo−S bond and in the respective valence ionization energies of sulfido versus thiolate donor ligands. As a result, the higher energy $S^{\sigma,\pi}_{sulfido} \rightarrow$ Mo charger transfer transitions are obscured by other strong absorptions and are not observed in oxidized XO or [(L-N_3)MoOS(OPh)]$^{5/6+}$ model complexes, as previously proposed.[16,31] The presence of a strong Mo−S π* interaction in the LUMO of oxidized XO, the putative e^- acceptor orbital in the reductive half-reaction, has been proposed to play a vital role in XO mediated hydroxylations.[31]

Conclusions. A combination of electronic absorption, MCD, and rR spectroscopies have been used to show that a strong Mo−S π-bonding interaction is present in complexes **1**−**4**. This covalent bonding interaction is the origin of the intense low-energy absorption feature that is characteristic of these complexes, and this transition is assigned as a $S^{v}_{180} \rightarrow$ Mo d_{xy} LMCT transition. Significantly, the strong π-type Mo $d_{xy}-S^{v}_{180}$ bonding interaction is analogous to the Cu $d_{x^2-y^2}-S^{v}_{Cys}$ bonding scheme observed for blue copper proteins, which also possess an intense ~16 000 cm^{-1} LMCT transition. Kinematic coupling of the Mo−S_{180} stretch with low-frequency modes of the L-N_2S_2 ligand is the likely origin of the complex rR spectra of **1**−**4**, which is very similar to the rR spectra of blue copper proteins. DFT calculations show that a strong π-type Mo $d_{xy}-S_{Cys}$ orbital interaction is not possible for the active site geometry of SO found by X-ray crystallography; however, rotation about the Mo−S_{Cys} bond during catalysis could create a more favorable orbital orientation for electron transfer or for modulating the reduction potential of the molybdenum center. Finally, for oxidized XO, the presence of a strong Mo═$S_{sulfido}$ π interaction, comparable to the Mo $d_{xy}-S^{v}_{180}$ bonding in complexes **1**−**4**, is indicated by the DFT calculations on a model for the active site.

Acknowledgment. Support of this research by the National Institutes of Health (Grant No. GM-057378 to M.L.K. and GM-37773 to J.H.E.) is gratefully acknowledged.

Supporting Information Available: Coordinates for the computational models in Table 2/Figure 7, mull absorption of **2**−**4** (Figure S1), a deconvoluted rR spectrum of **4** (Figure S2), Gaussian-resolved MCD and electronic absorbance spectra of **2** (Figure S3) and **3** (Figure S4), and a rR spectrum of (L-N_2S_2)MoOSePh (Figure S5). This material is available free of charge via the Internet at http://pubs.acs.org.

IC034206N

(93) Stiefel, E. I. *Pure Appl. Chem.* **1998**, *70*, 889.
(94) Lim, B. S.; Fomitchev, D. V.; Holm, R. H. *Inorg. Chem.* **2001**, *40*, 4257.
(95) Peariso, K.; Chohan, B. S.; Carrano, C. J.; Kirk, M. L. *Inorg. Chem.* **2003**, *42*, 6194.
(96) Terminal sulfido ligands have two S^{v} orbitals that are orthogonal to each other. The in-plane orbital forms the strong π bond with d_{xy} and is therefore referred to as S^{π}. The second sulfido S^{v} orbital is oriented orthogonal to d_{xy} akin to the $S_{90}{}^{v}$ and $S_{nc}{}^{v}$ orbitals.
(97) Ryan, M. G.; Ratnam, K.; Hille, R. *J. Biol. Chem.* **1995**, *270*, 19209.
(98) Thapper, A.; Donahue, J. P.; Musgrave, K. B.; Willer, M. W.; Nordlander, E.; Hedman, B.; Hodgson, K. O.; Holm, R. H. *Inorg. Chem.* **1999**, *38*, 4104.